DESIGN AND EXPERIMENTAL STUDY OF DIRECT-CONNECTED FOUR-WHEEL DRIVE TRANSMISSION SYSTEM FOR MICRO CULTIVATORS

, *直联式四驱微耕机传动系统设计与试验*

Heng ZHANG¹⁾, Yihan FANG¹⁾, Chen XUE ¹⁾, Lichao LIU *1,2)

¹⁾ College of Engineering, Anhui Agricultural University, Hefei, Anhui, 230036, China
²⁾ Engineering Laboratory of Intelligent Agricultural Machinery Equipment, Anhui, Hefei, 230036, China *Tel:* +86 15705603452; E-mail addresses: Ilchao@ahau.edu.cn
Corresponding author: Lichao Liu

DOI: https://doi.org/10.35633/inmateh-77-02

Keywords: Direct-connected 4WD system, Micro cultivators, Four-wheel drive transmission, Gear optimization

ABSTRACT

Addressing the critical challenge of energy efficiency loss in micro-cultivator transmission systems within China's hilly terrains, this study develops a direct-connected four-wheel-drive transmission system to enhance efficiency and reliability. Based on agronomic requirements and functional demands for gear positions, a combined gear-chain transmission scheme was implemented, enabling coordinated control between traveling and tilling units, supporting five operational modes, including fast/slow tillage and reverse gear. Through optimized gear parameters and structural configuration, along with carbonitriding treatment and microgeometry optimization of 20CrMnTi gears, the system achieves significantly improved load capacity and compactness. Integrated validation with KissSoft and Romax that gear safety factors exceed design targets, shaft and bearing lifespan meet the 1,000-hour requirement, and the simulated transmission efficiency of 92.2% surpasses conventional pulley systems. Field verification demonstrates 78.58% soil fragmentation and 90.20% tillage depth stability at a forward speed of 3.46 km/h with a ploughing depth of 22.93 cm, meeting agronomic standards for micro-cultivator operations. This research provides a technical reference for transmission system design in small hillside agricultural machinery.

摘要

针对中国丘陵山区微耕机传动系统存在能效损失的关键问题,本文设计了一种直联式四驱微耕机传动系统,旨在提升传动效率与可靠性。基于农艺要求与挡位功能需求,采用齿轮传动与链传动结合的方案,实现行走部分与旋耕部分的协同控制,支持快耕、慢耕、倒挡等 5 种工作模式。通过优化齿轮参数与结构布局,采用碳氮共渗强化齿轮与微几何优化技术提升齿轮承载能力与紧凑性。结合 KissSoft 与 Romax 软件对齿轮强度、轴疲劳安全系数及轴承寿命进行校核,结果表明:齿轮齿面与齿根安全系数均高于目标值,轴与轴承寿命满足设计要求,传动效率仿真达 92.2%,优于传统皮带轮传动系统效率。田间试验证实微耕机前进速度 3.46 km/h、耕深22.93 cm 时,碎土率 78.58%,耕深稳定性系数 90.20%,结果满足了微耕机耕作的农艺要求。本研究可为丘陵山区小型农机的传动系统设计提供技术参考。

INTRODUCTION

China's hilly and mountainous regions encompass 63.2% of the nation's total cultivated land area (*Li et al., 2022*). The micro-tiller, characterized by compact dimensions and operational simplicity, demonstrates strong adaptability for agricultural operations in these topographically complex areas, presenting broad application potential (*Peng et al., 2022, Yang et al., 2023, Wang et al., 2020*). As the core power transmission component, the gearbox critically determines micro-tiller performance through its transmission efficiency and durability, factors that directly influence tillage quality and operational costs for farmers (*Liu et al., 2022*). Current research primarily emphasizes structural optimization through algorithmic optimization approaches to achieve gearbox miniaturization (*Li et al., 2022*). However, international studies reveal that multi-axial loading conditions in hilly terrains still induce dynamic efficiency degradation in gear systems (*Liu et al., 2024*). These findings underscore the necessity of comprehensive consideration regarding transmission efficiency and service life during micro-tiller gearbox design phases.

Contemporary investigations into micro-tiller transmission systems bifurcate into structural innovation and volumetric optimization research streams. Zheng et al., (2025), developed a novel high-ratio transmission mechanism addressing limitations in conventional micro-tiller gear ratios to demonstrate enhanced ease of installation, which reduced failure rates and improved reliability. Xiao et al., (2024), performed numerical simulation analysis on the cutting performance of micro-tiller rotary blades using ANSYS and LS-DYNA software, conducting comparative optimization of cutting resistance and power consumption between forward and reverse rotating blade configurations. Yosef et al., (2024), established an SPH-FEM coupled modeling methodology advancing soil-implement interaction studies. Vu et al., (2024), optimized two-stage helical gearbox configurations, achieving equilibrium between dimensional reduction and efficiency enhancement through strategic parameter combination selection. Concurrently, Tobie et al., (2017), achieved a breakthrough in gear performance through innovative alloy technology implementation. Despite these advancements, belt-driven systems still exhibit significant energy losses under multi-axis loading conditions in hilly terrains, limiting transmission efficiency to below 85% in field operations (Kwon et al., 2023). Current micro-tiller configurations predominantly employ belt-driven engine-transmission connections, which suffer from circuitous power pathways and suboptimal efficiency, ultimately constraining operational economy.

To overcome these limitations, this research integrates agronomic requirements with micro-tiller-specific gear performance criteria to develop a direct-coupled four-wheel-drive transmission system. The proposed design targets a 1000-hour service life and exceeds 90% transmission efficiency. Through systematic theoretical analysis complemented by Romax simulation verification, gearbox longevity and efficiency parameters were established and subsequently validated through rigorous field testing of operational performance characteristics.

MATERIALS AND METHODS

Structure and working principle of the gearbox

The micro tillage machine designed in this paper selects a 186F single-cylinder air-cooled diesel engine as an engine, with a rated power of 6.3 kW and a rated speed of 3600 r/min. During fast tillage, the designed speeds at the end of the walking section and rotary tillage section are 42 r/min and 428 r/min, and the speeds at the end of the walking section and rotational speed during slow tillage are 19 r/min and 197 r/min. The gearbox scheme and three-dimensional model of the direct connection four-wheel drive micro-tiller gearbox are shown in Figure 1.

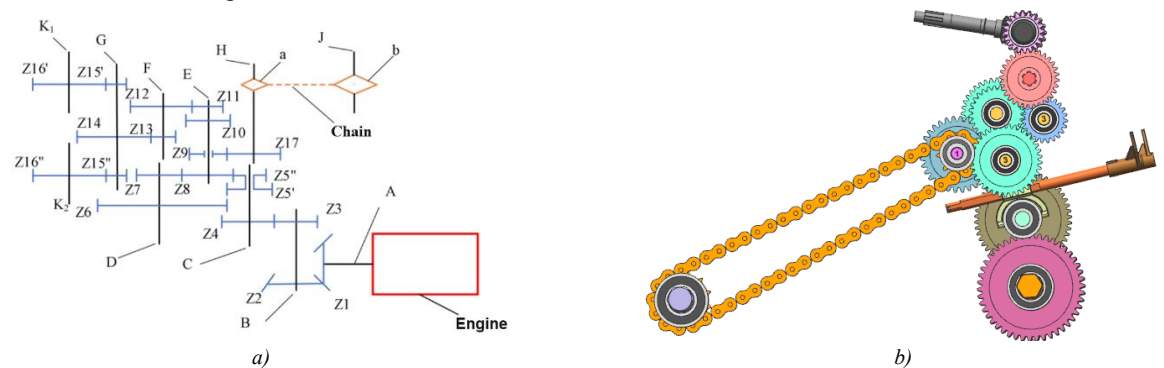


Fig. 1 – Gearbox scheme and 3D model of gearbox system
a) Transmission scheme; b) 3D model of the transmission

The gearbox is divided into the traveling section and the rotary tillage section, and the traveling section is equipped with four gears, namely, the traveling fast gear, the traveling slow gear, the reverse gear, and the traveling neutral gear. The rotary tillage section is set with two gears, namely the rotary tillage gear and the rotary tillage neutral gear. Through the combination of the traveling gear and the rotary tillage gear, a total of five working states can be achieved, namely fast tillage, slow tillage, reverse gear, forward gear, and neutral gear. It can adapt to the different functional requirements of rotary tillage operations and field transfer driving.

Design of transmission gears

Distribution of transmission ratio

The transmission ratios of each level in the transmission system have a significant impact on the size, center distance, and mass of the transmission mechanism.

Therefore, when the transmission ratio distribution of the transmission system is designed, the following requirements should be followed:

- 1. The gearbox has a compact structure.
- 2. The size and layout of each transmission component are reasonable, and no interference occurs.
- 3. The difference in transmission ratios between the adjacent two stages should not be too significant.
- 4. In gear transmission, the oil immersion of the large gear is reasonable.
- 5. The transmission ratio should not be rounded as much as possible.

During the design process, the single-stage gear transmission ratio is generally no more than 8, and the single-stage chain transmission ratio is generally no more than 10. The transmission ratio allocation for the entire machine is shown in Table 1.

The distribution of the transmission ratio

Table 1

	Fast tillage gear		Slow tillage gear		
	Rotary tillage	Walking	Rotary tillage	Walking	
	1.73	1.73	1.73	1.73	
	1.5	1.5	1.5	1.5	
Tuenemieelen vetie	1.21	1.21	2.64	2.64	
Transmission ratio	1.78	2.64	1.78	2.64	
	1.5 (Chain drive)	3.33	1.5 (Chain drive)	3.33	
	1	3.07	1	3.07	

The rotational speed and torque of each shaft can be calculated through the transmission ratio and engine parameters. The deceleration of the slow-till gear is relatively significant, and the torque received by each shaft is greater than that of the fast-till gear. Therefore, the rotational speed and torque of each shaft are calculated for the slow-till gear. When the gearbox is working, the power proportion between the rotary tillage shaft and the drive shaft varies with the working conditions. In this paper, the allocation of 80% of the engine power to the rotary tillage part is calculated. The parameter calculation formulas of each axis are shown in Eqs. 1 to 3.

$$n_B = n_A \cdot i_{AB} \tag{1}$$

$$P_{B} = P_{A} \cdot \eta \tag{2}$$

$$T_B = \frac{9550P_B}{n_B} \tag{3}$$

where: n_B is the rotational speed of the current transmission shaft (r/min); n_A represents the rotational speed of the transmission shaft of the previous stage (r/min); i_{AB} is the transmission ratio between the two shafts; P_B is the power of the current transmission shaft (kW); P_A represents the power of the transmission shaft of the previous stage (kW); η is the transmission efficiency; and T_B represents the torque of the current transmission shaft (N·m).

The dynamic parameters of each shaft in the slow gear obtained through calculation are shown in Table 2.

Dynamic parameters of each slow gear shaft

Table 2

Parameter	Shaft B	Shaft C	Shaft E	Shaft F	Shaft G	Shaft H	Shaft J	Shaft K
Rotational speed (r/min)	2084	1389	526	199	60	296	197	19
Power (kW)	6.11	5.93	5.75	1.12	1.08	4.47	4.24	0.5
Torque (N·m)	28	40.77	104.4	53.75	171.9	144.22	205.54	251.32

Design of transmission gears

Excessive contact stress on the tooth surface and at the tooth root during gear transmission can lead to tooth breakage and tooth surface wear failure of gears, thereby losing their transmission capacity (*Xu et al., 2023, Liu et al., 2020*). To reduce the size of the gearbox, the structure of the transmission system inside the gearbox should be as compact as possible. Meanwhile, to ensure the load-carrying capacity of the gears, measures such as reducing the tooth width, increasing the tooth thickness, and performing positive displacement on the pinion and negative displacement on the pinion of a pair of gears can be taken (*Yuan et al., 2021*).

According to the requirements of the transmission route, the gears (Z1 and Z2) are designed as bevel gears, with a tooth profile angle of 20°, a helix angle of 20°, and right-rotating. The remaining gears are all standard spur gears with a pressure Angle of 20°. The material is 20CrMnTi, and the surface treatment method is carburizing and nitriding. The surface hardness is HRC58-62, and the core hardness is HRC35-42. The calculation formulas for the gear modification coefficient and module refer to Eqs. 4 and 5.

$$x_{\min} = \frac{h_a \cdot (z_{\min} - z)}{z_{\min}} \tag{4}$$

$$x_{\min} = \frac{h_a \cdot (z_{\min} - z)}{z_{\min}}$$

$$m \ge 3\sqrt{\frac{Y_{FS}}{[\sigma_F]} \cdot \frac{2TK_F}{\varphi_a z^2}}$$
(4)

where: x_{min} is the coefficient of the minimum displacement; h_a represents the coefficient of the tooth top height, h_a =1; z_{min} is the minimum number of teeth, z_{min} =17; m is the modulus; K_F represents the load coefficient, K_F =1.6; T is the torque between gear pairs (N); $[\sigma_F]$ represents the allowable bending fatigue strength of gear materials (MPa), $[\sigma_F]$ =200; And φ_d represents the tooth width factor, φ_d =1.8.

Taking the Z3 and Z4 gear sets as examples, it is calculated that the minimum modification coefficient of Z3 is x_{min} =-0.17, the minimum modification coefficient of Z4 is x_{min} =-0.76, and the module m > 0.35. To ensure that the center distance does not change after modification, the modification coefficient of Z3 is taken as x_{Z3} =0.25, and the modification coefficient of Z4 is taken as x_{Z4} =-0.25. And the modulus(m) is 2.5. The parameters of each gear of the gearbox are shown in Table 3.

Table 3

Transmission gear parameters The Tooth The Tooth Gear Number Gear Number modulus displacement modulus displacement width width number of teeth number of teeth (mm) coefficient (mm) coefficient **Z**1 11 9.88 3 +0.25 **Z**9 18 12 3 -0.2510 9.88 28 2.5 +0.25 **Z**2 19 3 -0.25Z10 14 **Z**3 20 12 2.5 +0.25 Z11 14 2.5 -0.2512 12 **Z**4 30 2.5 -0.25 Z12 37 2.5 +0.25 Z5' 23 10 2.5 15 14 2.5 +0.25 Z13 -0.2512 Z5" 14 12 2.5 -0.25 Z14 50 2.5 +0.25 16 **Z**6 23 10 2.5 15 -0.35 +0.25 Z15 3 12 **Z**7 14 14 2.5 46 3 +0.35 -0.25Z16 12 12 32 3 Z8 37 2.5 +0.25 Z17 -0.25

The design of the drive shaft

The material of the drive shaft is selected as 20CrMnTi. The formula for estimating the minimum diameter of the shaft is as follows:

$$d \ge 3\sqrt{\frac{5}{[\tau_T]}} \times 9550000 \frac{P}{n} = M \ 3\sqrt{\frac{P}{n}}$$
 (6)

where: d is the coefficient of the minimum displacement; τ_T represents the coefficient of the tooth top height; P is the minimum number of teeth; n is the modulus; M represents the load coefficient.

Taking shaft B as an example. According to the rotational speed and power of shaft B listed in Table 2, taking M as 100 and substituting it into Eq. 6, the minimum diameter dB of shaft B is calculated to be 14.3mm. Therefore, the minimum shaft diameter of shaft B is taken as 17mm and is matched with the 6203 bearing. The minimum diameters of the remaining shafts and the matching bearings are shown in Table 4.

Axle diameters and bearing models

Table 4

	Axic didirects and bearing models							
Shaft name	Minimum shaft diameter(mm)	Bearing model	Shaft name	Minimum shaft diameter(mm)	Bearing model			
Shaft A	20	6204	Shaft F	17	6203			
Shaft B	17	6203	Shaft G	20	6304			
Shaft C	17	6203	Shaft H	17	6303			
Shaft D	17	6203	Shaft K	35	6007			
Shaft E	17	6203	Shaft J	35	6207			

Gear strength verification

Taking Z3 and Z4 as examples, the gear strength is checked using KissSoft software. In KissSoft, we select the cylindrical gear pair and input the basic geometric parameters of the gear, such as the number of teeth, tooth width, module, gear type, pressure angle, center distance, and modification coefficient. The 20CrMnTi and gear 1 are selected as the material type and the driving gear, and the rotational speed of Z3 is set at 2084/r/min and the power at 6.11kW. The gear life is set to 1000 hours. The calculation results are shown in Table 5. It can be seen that the contact stresses of Z3 and Z4 are 958.78MPa and 949.14MPa, respectively, and the root stresses of the teeth are 164.49MPa and 185.11MPa, respectively, all of which are less than the allowable stresses of the 20CrMnTi material gears calculated earlier. The tooth surface safety factors of Z3 and Z4 are 1.41 and 1.42, respectively, and the tooth root safety factors are 5.29 and 4.71, respectively, both of which are greater than the target safety factors of 1.0 and 1.4. Therefore, the gear strength meets the design requirements.

Table 5
Gear strength analysis data

Gear Strength analysis data							
Gear number	Tooth surface contact stress (N • mm²)	Safety factor of tooth surface contact stress	Tooth root stress (N • mm²)	Safety factor of tooth root stress			
Gear 1	958.87	1.41	164.49	5.29			
Gear 2	948.15	1.42	185.11	4.71			

The strength check results of the remaining gear sets are shown in Table 6. It can be seen that the safety factor of the tooth surface and the safety factor of the tooth root of each gear set are both greater than that of gear 1, that is, the failure probability of the gears within the set 1000h usage time is less than 1%. Therefore, it is considered that the design of the gear parameters of the gearbox meets the requirements of the service life.

Table 6
Gear strength check

	Tooth surface strength Tooth root strength		Tooth surface strength		ace strength	Tooth root strength			
Gear	Contact stress (MPa)	Safety coefficient	Tooth root stress (MPa)	Safety coefficient	Gear	Contact stress (MPa)	Safety coefficient	Tooth root stress (MPa)	Safety coefficient
Z1	1187.28	1.26	153.89	5.63	Z9	1132.24	1.10	331.56	2.71
Z2	1207.36	1.28	146.82	5.95	Z10	1085.84	1.12	259.31	3.39
Z3	958.78	1.41	164.49	5.29	Z11	1092.39	1.17	174.15	5.15
Z4	949.14	1.42	185.11	4.71	Z12	1033.94	1.20	181.66	5.02
Z5'	1082.52	1.12	227.61	3.88	Z13	1188.70	1.02	322.04	2.84
Z5"	1163.81	1.09	321.52	2.74	Z14	1180.85	1.02	385.87	2.43
Z 6	1177.96	1.07	273.31	3.20	Z15	1498.26	1.00	477.51	1.52
Z 7	1162.64	1.09	267.81	3.29	Z16	1325.37	1.01	452.68	1.71
Z8	1185.49	1.05	335.38	2.67	Z17	1341.44	1.02	361.63	2.50

Simulation verification of the transmission system based on Romax

The establishment of the Romax model

As shown in Figure 2, the intermediate shaft A is the input shaft for power, the left side is the rotary tillage output shaft J, and the right side is the drive output shaft K. We set the power load input point (input) on axis A and set one power load output point (rotary tillage load 1 and rotary tillage load 2) at each end of axis J. Meanwhile, setting one power output load point (drive load 1 and drive load 2) at each end of axis K is indispensable. When the high gear is set, the Z10 clutch is locked. And when we set the low gear, the Z11 clutch is closed.

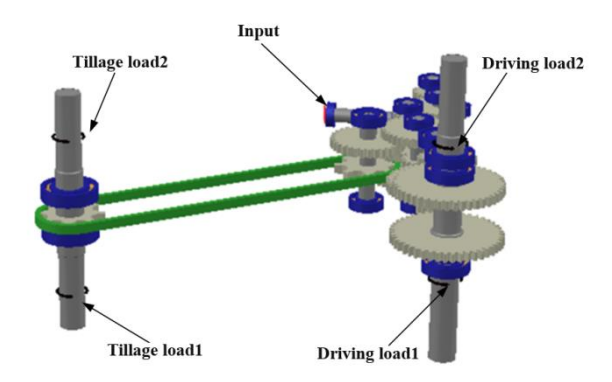


Fig. 2 - Field experiment results

During the operation of the micro-tiller, the power consumption of the rotary tillage part is approximately 80% of the total power consumption. The power at each rotary tillage power output load point is set to -2.52kW, and the symbol indicates the output of the load. Romax itself calculates the load of the drive part, and the engine parameters determine the power input load point. The input load is 6.3kW, and the rotational speed is 3600/rpm. After submitting the calculated power flow, the load point operating condition data at each gear position are shown in Table 7. Reverse gear and neutral gear are not considered.

Power flows at the load points at each gear

Table 7

		•		
Gear position	Load point	Power(kW)	Torque(N·m)	Speed(rpm)
	input	6.3	16.71	3600
	Rotary tillage load 1	-2.52	-56.23	428
Fast gear	Rotary tillage load 2	-2.52	-56.23	428
	Driving load 1	-0.67	-151.52	42
	Driving load 2	-0.59	-133.28	42
	input	6.3	16.71	3600
	Rotary tillage load 1	-2.52	-122.16	197
Slow gear	Rotary tillage load 2	-2.52	-122.16	197
	Driving load 1	-0.67	-331.91	19
	Driving load 2	-0.59	-286.35	19

Shaft strength verification

The shaft is an indispensable part of the transmission to support components such as gears and clutches. When the shaft is in operation, it will be subjected to various impact forces, vibrations, bending moments, and torques. When the strength and rigidity of the shaft are insufficient, bending deformation will occur, which will affect the gear meshing. In severe cases, it may cause gear damage, reducing the performance and service life of the gears. Therefore, when designing the shaft, it is necessary to check the strength of the shaft (Baglioni et al., 2012). The strength verification of a shaft is usually judged by calculating the fatigue safety factor at its dangerous sections to determine its reliability. The verification formula for the safety factor S of dangerous sections is as follows:

$$S = \frac{S_{\tau}S_{\sigma}}{\sqrt{S_{\sigma}^2 + S_{\tau}^2}} \ge S_p \tag{7}$$

where: S_{τ} is the safety coefficient during torsion; S_{σ} represents the safety coefficient during bending; S_{p} is the allowable safety factor.

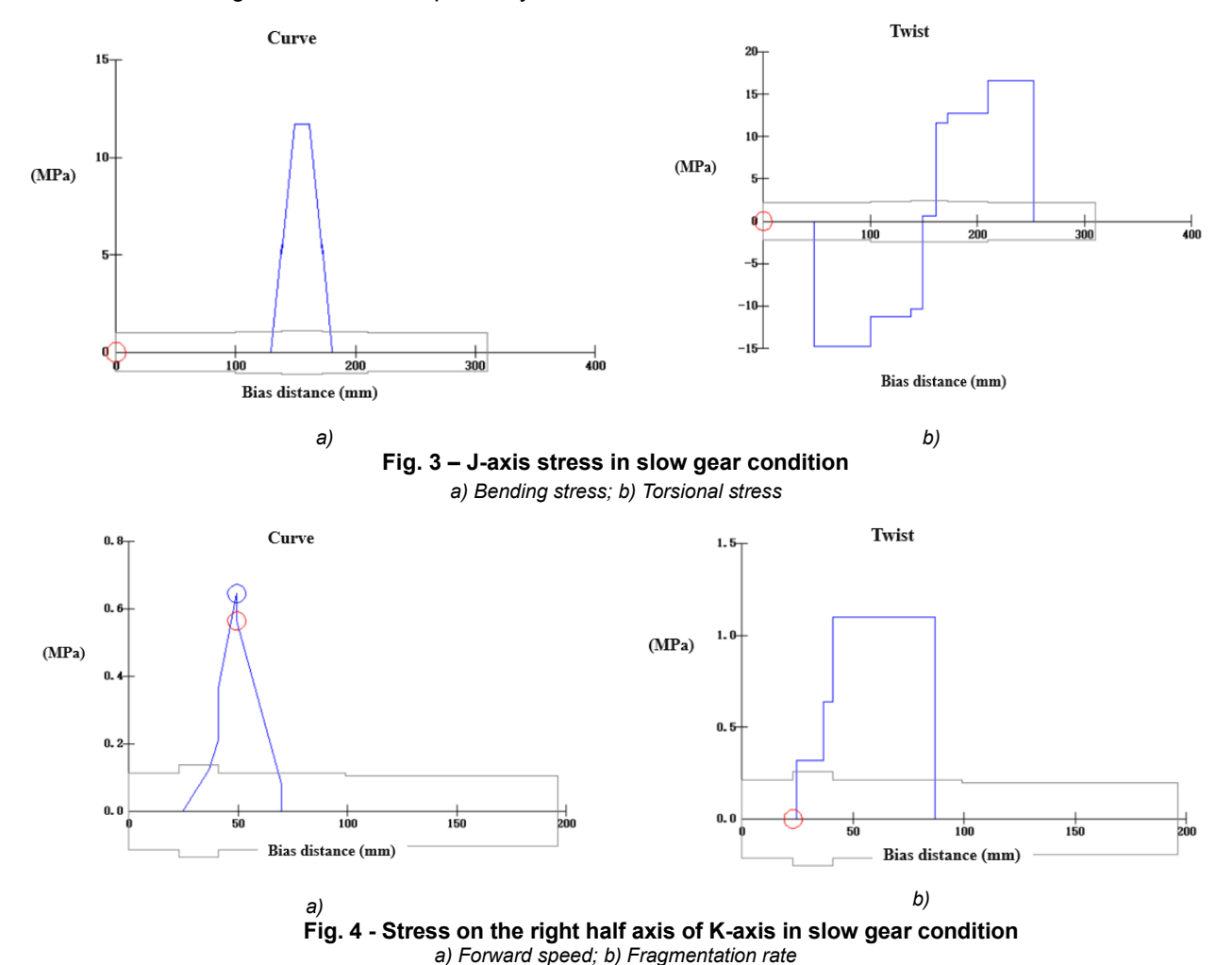
$$S_{\tau} = \frac{\tau_{-1}}{\frac{K_{\tau}\tau_{a}}{\beta\varepsilon_{\tau}} + \varphi_{\tau}\tau_{m}} \tag{8}$$

$$S_{\tau} = \frac{\tau_{-1}}{\frac{K_{\tau}\tau_{a}}{\beta\varepsilon_{\tau}} + \varphi_{\tau}\tau_{m}}$$

$$S_{\sigma} = \frac{\sigma_{-1}}{\frac{K_{\sigma}\sigma_{a}}{\beta\varepsilon_{\alpha}} + \varphi_{\sigma}\sigma_{m}}$$
(8)

where: τ_{-1} is the torsional fatigue limit of materials (MPa); σ_{-1} represents the bending fatigue limit of materials (MPa); K_{τ} , K_{α} are the effective stress concentration coefficients during torsion and bending; β represents the surface quality coefficient of the material; ε_{τ} , ε_{α} is the dimensional coefficients during torsion and bending; φ_{τ} , φ_{α} represents the average stress conversion coefficient for torsion and tension of materials; τ_{α} , τ_{m} represents the torsional stress range and average stress (MPa); and σ_{a} , σ_{m} represents the bending stress range and average stress.

Due to the large number of transmission shafts in the transmission system and the complex working conditions, the shaft verification analysis takes the power load output shafts J and K in the slow gear situation as examples, and the K shaft is analyzed as the right half shaft. The verification results of the J-axis and K-axis are shown in Figures 3 and 4, respectively.



It can be seen from Figure 3 that the bending stress at the installation of the J-axis gear is the greatest one, with a magnitude of 11.7MPa. The maximum value of the absolute value of torsional stress occurs at the two load output points, with a magnitude of 16.36 MPa. It can be seen from Figure 4 that the peak bending stress of the K-axis is at the left end face of the first bearing, with the bending stress magnitude of 0.64MPa and a maximum torsional stress of 1.09MPa, which is located at the output load point.

It can be obtained through calculation that $\tau_{Ja}=\tau_{J\max}/2=8.18MPa$, $\tau_{Jm}=\tau_{Ja}=8.18MPa$, $\sigma_{Ja}=\sigma_{J\max}/2=5.85MPa$, $\sigma_{Jm}=\sigma_{Ja}=5.85MPa$, $\tau_{Ka}=\tau_{K\max}/2=0.55MPa$, $\tau_{km}=\tau_{ka}=0.55MPa$, $\sigma_{Ka}=\sigma_{K\max}/2=0.32MPa$, $\sigma_{m}=\sigma_{a}=0.32MPa$.

The material of the transmission shaft is selected as 20CrMnTi. Other parameters obtained by referring to the mechanical design manual are shown in Table 8.

Table 8

A vial	strength	check	parameters
ANIAI	3u chuun	CHECK	Dai ailietei 3

$\sigma_{\scriptscriptstyle{-1}}$	$ au_{-1}$	K_{σ}	$K_{ au}$	\mathcal{E}_{σ}	$\mathcal{E}_{ au}$	$arphi_{\sigma}$	$arphi_{ au}$	β
525	300	1.73	2.71	0.83	0.89	0.34	0.21	8.0

From Eq. 8 and Eq. 9, we obtain $S_{J\tau}$ = 9.13, $S_{J\sigma}$ =30.47, $S_{K\tau}$ =135.81 and $S_{K\sigma}$ =557. Substituting it into Eq. 7, we can obtain E=5 and F=6. It can be known that the fatigue strength safety factors of the J-axis and the K-axis are much greater than the allowable fatigue strength safety factor, and the J-axis and the K-axis meet the fatigue strength requirements.

Bearing life verification

When the gearbox is in operation, the bearings are subjected to periodic loads. The metal material on the contact surface between the balls and the raceways will generate periodic shear stress. When the cycle period reaches a certain number of times, the metal will become fatigued and thus fail. In this paper, the ISO281 standard is adopted for the life verification of bearings, and the life calculation formula is shown in Eq.10.

$$L = \delta_1 \delta_2 \delta_3 \left(\frac{C}{P}\right)^{\varepsilon} \tag{10}$$

where: L is the bearing life, h; C represents the rated dynamic load (MPa); P is the equivalent dynamic load (MPa); ε is the life parameters (for roller bearings, take 10/3; for ball bearings, take 3); δ_1 represents the reliability coefficient; δ_2 is the material coefficient; δ_3 represents the using conditional coefficient.

The fatigue life of each bearing in the gearbox is calculated using the ISO281 standard. Figure 5 shows the computed bearing lives of all bearings. It can be seen from the figure that the rolling bearings 8 and 9 on the E shaft have relatively low lives, which are 3962 hours and 2186 hours, respectively, both exceeding the design life of 1000 hours for the micro-tiller. The lives of the remaining bearings are all greater than 6000 hours. Judging from the life values, the bearing lives meet the usage requirements.

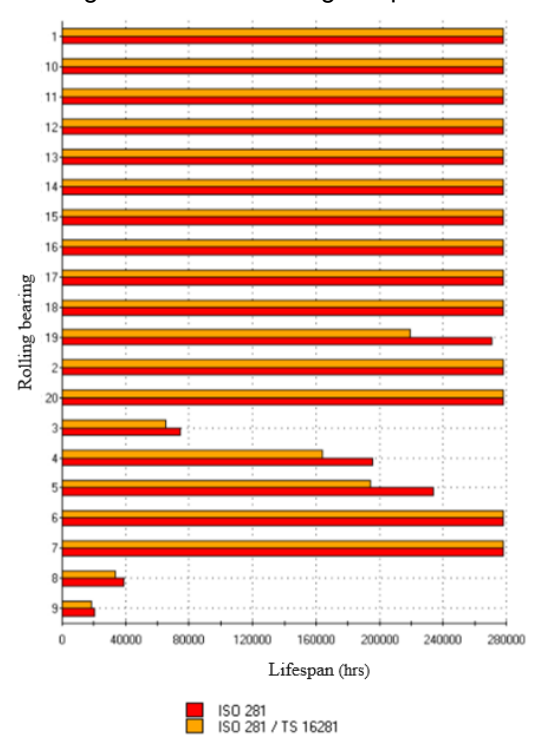
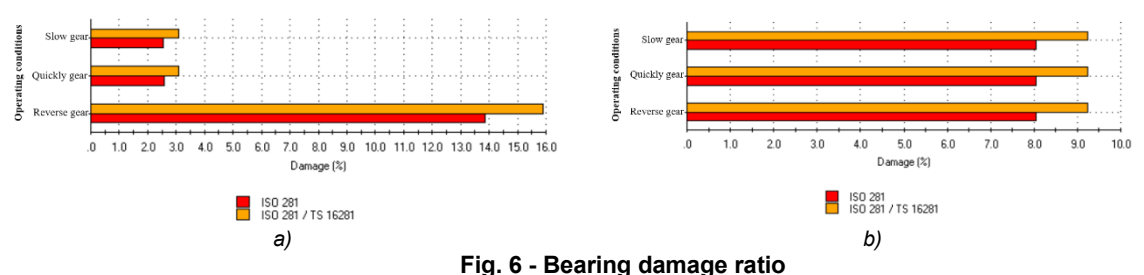


Fig. 5 - Calculation results of bearing life

Figure 6 shows the damage fatigue ratios of rolling bearings 8 and 9 under three working conditions. The red bar chart represents the ratio between the defined load duration (1000h) and the calculated bearing life, and the yellow bar chart illustrates the damage ratio calculated after automatic correction by the Romax software.

The red damage ratio is obtained without considering external factors and internal factors of the bearing, and has little reference value. The yellow damage ratio is closer to the actual situation. Suppose the difference between the red damage ratio and the yellow damage ratio is too significant. In that case, it indicates that the structure of the shaft at this location needs to be optimized. Suppose the difference between the red damage ratio and the yellow damage ratio is not large, but the damage ratio exceeds 100%. In that case, it indicates that the bearing's load-carrying capacity is insufficient and the bearing needs to be replaced. It can be seen from Figure 6 that the damage ratios of rolling bearing 8 and rolling bearing 9 under the three working conditions are all less than 100%, and the difference between the red damage ratio and the yellow damage ratio is slight, indicating that the bearings are sufficient to bear the loads under the three working conditions.



a) Rolling bearing 8 damage ratio; b) Rolling bearing 9 damage ratio

Analysis of gear contact state

The studies show that reducing the static transmission error of gears can reduce the vibration and noise during gear transmission. Gear modification is divided into two types: tooth profile modification and tooth direction modification. It can effectively reduce the static transmission error of gears and improve the dynamic performance of gear transmission (*Abruzzo et al., 2023*).

In the interface of the analysis results of the microscopic geometric dimensions of gears in Romax, the analysis results of the contact stress at the gear end face can be derived. Figure 7 shows the load distribution on the tooth surface of Z17 when the Z17-Z9 gear set is in slow gear. It can be seen from the figure that the maximum contact stress on the tooth surface of Z17 is 1591MPa, and the linear transmission error reaches $4.26~\mu$ m, resulting in an uneven distribution of the contact stress on the tooth surface. The contact stress on the left tooth surface is much greater than that on the right. Excessive contact stress on the tooth surface can cause pitting on the gear tooth surface, while excessive linear transmission error will lead to uneven wear of the gear tooth surface and accelerate gear wear (*Bugaru et al.*, 2004).

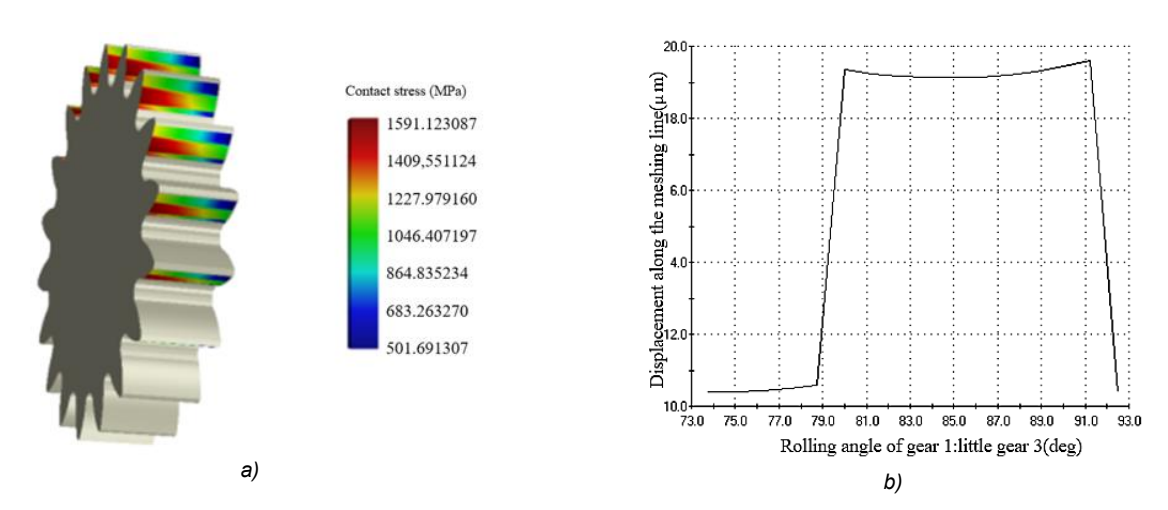


Fig. 7 - Microscopic geometric analysis of Z17
a) Maximum contact stress on the tooth surface; b) Linear transmission error

Aiming at the phenomenon that the current transmission error of the Z17 gear is significant and the maximum contact stress on the tooth surface is too substantial, the gear modification and optimization of the right tooth surface of the Z17 gear are carried out in Romax.

Z17 gear modification results

Table 9

Tooth tip	Involute	Involute drum	Tooth	The teeth are drum-
trimming(µm)	slope(µm)	shape(µm)	slope(µm)	shaped (µm)
1.08	10.53	23.88	10.42	0.004

The parameters of the modified Z17 gear were applied to the working conditions, and the microscopic geometric analysis of the Z17-Z9 gears was re-conducted. The results are shown in Figure 8.

It can be seen from the figure that after the modification, the maximum contact stress on the tooth surface of Z17 is 1345MPa, which is reduced by 15.5%. The linear transmission error is $3.44\mu m$, which is reduced by 19.2%. The maximum contact stress on the tooth surface is consistent in magnitude along the tooth thickness direction, and the modification effect of the tooth surface is apparent.

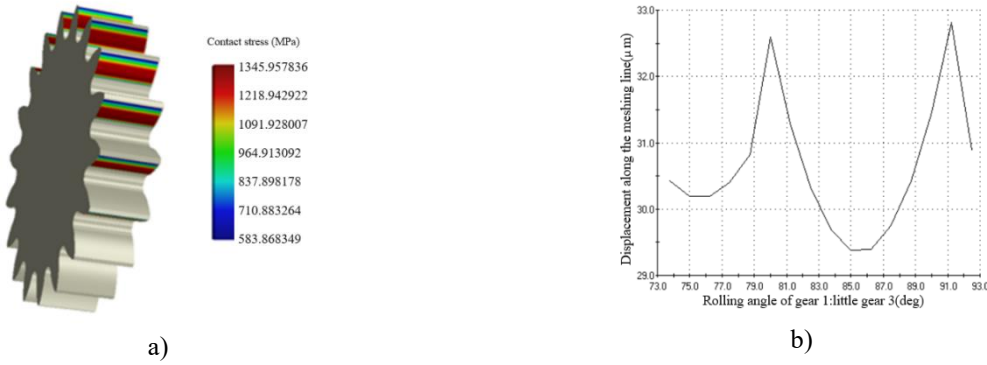


Fig. 8 - Microscopic geometric analysis of Z17 after modification a) Maximum contact stress on the tooth surface; b) Linear transmission error

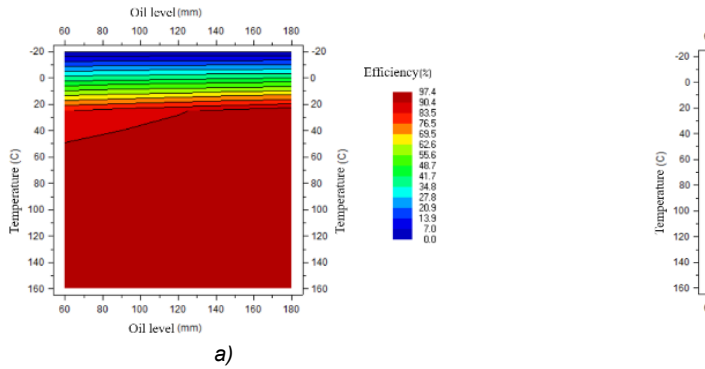
Verification of the transmission efficiency of the gearbox

The power loss during the transmission process of a gearbox is divided into gear meshing loss, bearing friction loss, and oil stirring loss. The efficiency calculation models include ISO14179-1, ISO14179-2, Anderson, SKF, etc. Among them, during the meshing process of a pair of gears, the meshing point is always on the common tangent of the two base circles. The efficiency of gear transmission is the average value of the transmission efficiency at the meshing point. The transmission efficiency of bearings is related to factors such as the bearing model, lubrication method, type of lubricant, load, and rotational speed (Gu et al., 2023). In actual working conditions, due to the difficulty in clearly calculating the transmission efficiency of bearings, empirical values are often directly used. In this paper, a pair of bearing transmission efficiencies $\eta_2 = 0.99$ is uniformly taken.

Oil stirring loss is the power loss caused by the friction between the parts in the transmission and the lubricating oil. The ISO 14719-1 standard classifies the causes of oil stirring loss into three types: loss caused by the smooth outer diameter of the parts, loss caused by the soft side of the parts, and loss caused by the gear teeth on the surface of the parts (*Mastrone et al., 2020*). In the subsequent calculations of this paper, the total crude stirring loss power is taken as 0.5% of the input power; its efficiency is $\eta_3 = 0.995$.

Transmission efficiency analysis

Romax is equipped with two transmission efficiency calculation models, ISO 14179-1 and ISO 14179-2. Through the calculation of gear meshing power loss, bearing friction power loss, and oil stirring power loss during the transmission process, the transmission efficiency of the gearbox can be estimated more accurately. After setting the working conditions, the type of lubricating oil, and the oil level, the transmission efficiency simulation can be carried out. Figure 9 shows the transmission efficiency of the directly connected gearbox and the pulley gearbox, as well as the influence of the lubricating oil level and working temperature on the transmission efficiency. It can be seen from the figure that the transmission efficiency increases with the rise of the working temperature and the lubricating oil level. When the working temperature is 25°C and the lubricating oil height is 60mm, the transmission efficiency of the directly connected gearbox is 92.2%, which is higher than the design requirement of 90%, and has a significant improvement compared with the 85.3% transmission efficiency of the same type of pulley drive gearbox.



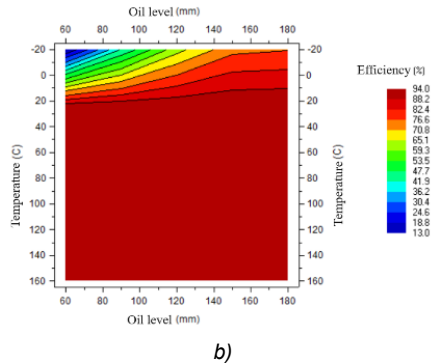


Fig. 9 - Two transmission efficiencies
a) Pulley transmission; b) Directly connected transmission

RESULTS

Field experiment

To verify the function and reliability of the transmission, a direct-connected four-wheel drive micro-tiller was assembled based on the transmission designed in this paper, and field tests were conducted. Referring to the performance requirements for micro-tillers in the "Outline for the Promotion and Appraisal of Agricultural Machinery" and GB/T5668-2017 "Rotary Tiller", the tests were carried out in the Nongcui Garden of Anhui Agricultural University in April 2024.

Gear shifting and steering functions.

By observing the operation status of the micro-tiller, it is concluded that there is no abnormal noise from the transmission during the gear shifting process of driving, the driving process is smooth, and the steering operation can be achieved through the control handle. The steering system function is normal.

Performance test of micro-tiller

By the performance requirements for micro-tillers in the "Outline for the Promotion and Appraisal of Agricultural Machinery", a test area of $30m \times 2m$ is set up, with a preparation area of 5m each in the front and back and a stabilization area of 20m in the middle. After completing the rotary tillage operation, the forward speed, tillage depth, tillage depth stability coefficient, soil fragmentation rate, and post-tillage flatness and other data were measured respectively. The test and measurement process is shown in Figure 10. Table 11 demonstrates that the micro-tiller's performance metrics—including a ploughing depth of 22.93 cm, post-plowing flatness of 4.0 cm, tillage stability coefficient of 90.2%, and soil fragmentation rate of 78.58%—fully comply with established agronomic requirements ($Qin\ et\ al.,\ 2016$).



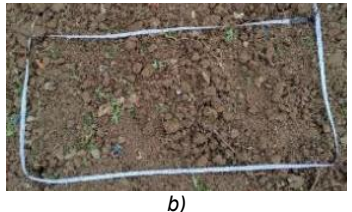


Fig. 10 - Field experiment results a) Forward speed; b) Fragmentation rate

Table 10

Performance test results of the micro-cultivator

Parameters	Forward speed (km·h ⁻¹)	Depth of cultivation(cm)	Tillage depth stability coefficient	Soil fragmentation rate	Post-plowing flatness(cm)
Results	3.46	22.93	90.2%	78.58%	4.0

CONCLUSIONS

- (1) A direct connection four-wheel drive micro-tiller transmission system is designed, adopting a combination of gear transmission and chain transmission to achieve coordinated control of the traveling part and the rotary tillage part, supporting five working modes including fast tillage, slow tillage, and reverse gear.
- (2) The service life of the transmission components is verified by combining KissSoft and Romax software. The gears, shafts, and bearings all met the 1000h service life requirement. The influencing factors of the transmission efficiency of the gearbox were analyzed. The transmission efficiency of the direct-connected gearbox and the belt-driven gearbox is analyzed and compared using the Romax software.

The simulation results show that the transmission efficiency of the direct-connected gearbox is 92.2%, which is 6.9% higher than that of the pull-driven gearbox.

(3) Field experiments show that the directly connected gearbox can achieve the straight-line driving, gear switching, and steering functions of the micro-tiller. When the forward speed is 3.46km/h and the ploughing depth is 22.93cm, the tillage depth stability coefficient is 90.2%, the soil fragmentation rate is 78.58%, and the flatness after ploughing is 4.0cm. The working performance meets the requirements of the national standard.

ACKNOWLEDGEMENT

This work was supported by the science and technology program projects of Anhui province and Wuhu city. No.2023n06020042 and 2023ly10.

REFERENCES

- [1] Abruzzo, M., Beghini, M., Santus, C., Presicce, F. (2023). A dynamic model combining the average and the local meshing stiffnesses and based on the static transmission error for spur gears with profile modification. *Mechanism and Machine Theory*, Vol.180, 105139
- [2] Baglioni, S., Cianetti, F., Landi, L. (2012). Influence of the addendum modification on spur gear efficiency. *Mechanism and Machine Theory*, Vol. 49, 216-233.
- [3] Bugaru, M. (2004). Chaotic Behavior of Helical Gear-Pair Systems Non-linear Parametrically Excited. *Rom. J. Acoust. Vib*, Vol.1, 7-13.
- [4] Gu, Y., Zheng, G. (2023). Dynamic evolution characteristics of the gear meshing lubrication for vehicle transmission system. *Processes*, Vol. 11, Issue 2, 561.
- [5] Kwon, K., Lee, J. H., Lim, S. K. (2023). Optimization of multi-speed transmission for electric vehicles based on electrical and mechanical efficiency analysis. *Applied Energy*, Vol. 342, 121203.
- [6] Li, H., Chen, L., Zhang, Z. (2022). A study on the utilization rate and influencing factors of small agricultural machinery: Evidence from 10 hilly and mountainous Provinces in China. *Agriculture*, Vol. 13, Issue 1, 51.
- [7] Li, X., Zhu, L., Gong, S. (2022). Soil-cutting simulation and dual-objective optimization on tillage process parameters of micro-tiller by smoothed particle Galerkin modeling and genetic algorithm. *Computers and Electronics in Agriculture*, Vol. 198, 107021.
- [8] Liu, H., Liu, H., Zhu, C., Tang, J. (2020). Study on gear contact fatigue failure competition mechanism considering tooth wear evolution. *Tribology International*, Vol.147, 106277.
- [9] Liu, X., Hao, W., Chen, Y., Hao, Q., Zhang, X., Sun, Z. (2024). Development of Vertical Vibration Model for Micro-Tiller by Smoothed Particle Hydrodynamics Method. *AgriEngineering*, Vol. 6, Issue 3.
- [10] Liu, X., Wang, Y., Zhang, X., Tian, H, Yu, F. (2022). Handheld Micro tiller time-frequency characteristic and vibration isolation measures. *Journal of Vibroengineering*, Vol. 24, Issue 5, 824-835.
- [11] Mastrone, M. N., Hartono, E. A., Chernoray, V., Concli, F. (2020). Oil distribution and churning losses of gearboxes: Experimental and numerical analysis. *Tribology International*, Vol. 151, 106496.
- [12] Peng, J., Zhao, Z., Liu, D. (2022). Impact of agricultural mechanization on agricultural production, income, and mechanism: evidence from Hubei province, China. *Frontiers in Environmental Science*, Vol. 10, 838686.
- [13] Qin, K., Ding, W., Fang, Z., Du, T., Zhao, S., Wang, Z. (2016). Analysis and experiment of tillage depth and width stability for plowing and rotary tillage combined machine. *Transactions of the Chinese Society of Agricultural Engineering*, Vol.32(9), 1-8.
- [14] Tobie, T., Hippenstiel, F., Mohrbacher, H. (2017). Optimizing gear performance by alloy modification of carburizing steels. *Metals*, Vol. 7, Issue 10, 415.
- [15] Vu, D. B., Tran, H. D., Dinh, V. T., Vu, D., Vu, N. P., Nguyen, V. T. (2024). Solving a Multi-Objective Optimization Problem of a Two-Stage Helical Gearbox with Second-Stage Double Gear Sets Using the MAIRCA Method. *Applied Sciences*, Vol. 14, Issue 12, 5274.
- [16] Yang, H., Ma, W., Liu, T., Li, W. (2023). Assessing farmland suitability for agricultural machinery in land consolidation schemes in hilly terrain in China: A machine learning approach. *Frontiers in plant science*, Vol. 14, 1084886.
- [17] Wang, Y., Li, X., Xin, L., Tan, M. (2020). Farmland marginalization and its drivers in mountainous areas of China. *Science of the Total Environment*, Vol. 719, 135132.

- [18] Wusong, X., Po, N., Pan, W., Yingjie, X., Fei, X. (2024). Simulation analysis and optimization of soil cutting of rotary blade by ANSYS/LS-DYNA. *INMATEH-Agricultural Engineering*, Vol. 72, Issue 1, 22–32. DOI: https://doi.org/10.35633/inmateh-72-02
- [19] Xu, F., Ding, N., Li, N., Liu, L., Hou, N., Xu, N., Chen, X. (2023). A review of bearing failure modes, mechanisms and causes. *Engineering Failure Analysis*, Vol. 152, 107518.
- [20] Yosef, T.Y., Fang, C., Faller, R.K., Kim, S., Bielenberg, R.W., Stolle, C.S., Pajouh, M.A. (2024). Adaptive coupling of FEM and SPH method for simulating dynamic post-soil interaction under impact loading. *Advances in Engineering Software*, Vol. 195, 103707.
- [21] Yuan, B., Liu, G., Yue, Y., Liu, L., Shen, Y. (2021). A novel tooth surface modification methodology for wide-faced double-helical gear pairs. *Mechanism and Machine Theory*, Vol. 160, 104299.
- [22] Zheng, S., Lu, T., Liu, J., Tian, Y., Han, M., Tai, M., Zhao, Z. (2025). Discrete Element-Based Design of a High-Speed Rotary Tiller for Saline-Alkali Land and Verification of Optimal Tillage Parameters. *Agriculture*; Basel, Vol. 15, Issue 3.